Available online at www.sciencedirect.com
ScienceDirect
Proceedings of the Combustion Institute 31 (2007) 1575–1582
Proceedings of the Combustion Institute
www.elsevier.com/locate/proci

Vortex-coupled oscillations of edge diffusion flames in coflowing air with dilution

Fumiaki Takahashi [a,*], Gregory T. Linteris [b], Viswanath R. Katta [c]

[a] National Center for Space Exploration Research on Fluids and Combustion, NASA Glenn Research Center, Cleveland, OH 44135, USA
[b] Fire Research Division, National Institute of Standards and Technology, Gaithersburg, MD 20899, USA
[c] Innovative Scientific Solutions, Inc., Dayton, OH 45440, USA

Abstract

The unsteady characteristics of oscillating methane diffusion flames in coflowing air diluted with CO_2 in earth gravity have been studied experimentally and computationally. The measured frequency of flame flickering due to buoyancy-driven large-scale vortices was bi-modal; it jumped from ≈11 Hz to ≈15 Hz with an increase in the air velocity (at ≈11 cm/s). As CO_2 was added into coflowing air gradually, the base (edge) of the flame detached from the burner rim, oscillated at half the flickering frequency, and blew off eventually. Numerical simulations with full chemistry predicted the internal flame structure and unsteady flame behavior: flame flickering, tip separation, base detachment, oscillation, and blowoff, in good agreement with the experiment. The mechanism of the edge diffusion flame oscillation was due to a cyclic series of events: (1) flame-base detachment and drifting downstream as a result of weakening due to dilution and a momentary increase in the entrainment-flow velocity associated with the vortex evolution, (2) fuel–air mixing in widened, lower-speed, wake space between the flame base and the burner rim, and (3) flame-base propagation through the flammable mixture layer back to the burner rim. A peak reactivity spot (reaction kernel) at the edge diffusion flame controlled the unsteady behavior through its dramatic changes in characteristics from the passively drifting to (premixed-type) propagating phase during a cycle. Because a mixing time of approximately 100 ms was required before propagation was enabled, a subsequent vortex evolved and passed. Thus, the flame-base oscillation was strongly coupled with the buoyancy-driven vortex evolution and the oscillation frequency was locked-in to half the flame-flickering frequency. The results have implications in turbulent flame structure; more specifically, the local extinction–mixing–reignition processes, in that the slow molecular mixing can become rate-limiting and the edge diffusion flame structure can be significantly different, depending on the phase in the process.

Keywords: Edge diffusion flame; Vortex–flame interaction; Flame oscillation; Flame flickering; Cup burner

1. Introduction

In turbulent diffusion flames, composed of ensembles of wrinkled, moving, laminar, diffusion-flame sheets, or flamelets [1], edges of diffusion flames can be formed as a result of local

* Corresponding author. Fax: +1 216 433 3793.
E-mail address: Fumiaki.Takahashi@grc.nasa.gov (F. Takahashi).

1540-7489/$ - see front matter © 2006 The Combustion Institute. Published by Elsevier Inc. All rights reserved.
doi:10.1016/j.proci.2006.07.227

extinction due to high strain rates, unsteady vortex–flame interactions, or suppression by fire-extinguishing agents. The edge diffusion flames may further extinguish toward global extinction, recede with a flow leading to blow-off, or if there is a sufficiently long fuel–air mixing time, propagate through the flammable mixture layer to merge with each other. Flame–surface interactions in fires over condensed materials also result in edge diffusion flames. Therefore, understanding of the unsteady behavior of edge diffusion flames is of fundamental and practical importance in both combustion systems and fires.

In recent years, low-frequency (a few Hz) oscillations of the edge of lifted jet diffusion flames have been reported by several researchers [2–11]. Different oscillation mechanisms of edge diffusion flames have been reported: the intrinsic pulsating instability near extinction in diffusion flames [4,6,9], buoyancy-driven oscillation due to Kelvin–Helmholtz instability in nozzle-attached diffusion flames [3,7], and the out-of-phase responses between the total burning rate and the buoyancy-induced convection in lifted diffusion flames [8,10,11]. The internal structure of an edge diffusion flame and its role in oscillations remain unknown.

By computations with a detailed reaction mechanism, the authors [12] have revealed that whether the edge diffusion flame became the triple flame structure is fuel-type dependent: acetylene and ethylene form the triple flame structure, but for alkanes (methane, ethane, and propane) the flame's rich branch nearly merges with the trailing diffusion flame. Furthermore, if a sufficiently long fuel–air mixing time (e.g., 0.3 s) is available, the edge diffusion flame propagates at the laminar burning velocity of stoichiometric mixtures through the flammable mixture layer. In the recent flame-suppression studies [13–15] using a cup-burner [16], a periodic oscillation of the edge diffusion flame was observed just prior to blowoff. Such flames provide well-controlled conditions suitable to investigate the mechanisms of edge diffusion flame oscillation and stabilization. This paper reports the experimental and numerical results of the unsteady edge-oscillation behavior and internal structure of a buoyancy-controlled methane diffusion flame in coflowing air diluted with CO_2 using the cup-burner configuration.

2. Experimental procedures

The burner, described previously [13–15], consists of a cylindrical glass cup (28 mm outer diameter, 45°-chamfered inside burner rim) positioned inside a glass chimney (85 mm inner diameter). To provide uniform flow, 6 mm glass beads fill the base of the chimney, and 3 mm glass beads (with two 15.8 mesh/cm screens on top) fill the fuel cup. Gas flows are measured by mass flow controllers (Sierra 860[1]) which are calibrated so that their uncertainty is 2% of indicated flow. The burner rim surface temperature, measured 3.7 mm below the exit using a surface temperature probe after running the burner for ≈10 min, was (514 ± 10) K.

The fuel used is methane (Matheson UHP, 99.9 %), and the diluent is carbon dioxide (Airgas, 99.5%). The air is house compressed air (filtered and dried) which is additionally cleaned by a filter (0.01 μm), a carbon filter, and a desiccant bed. The agent is added while holding a constant coflow (air + inert) velocity at 10.7 cm/s and a mean fuel velocity at 0.92 cm/s. The flame-flickering frequency is measured by a photodiode and lens which image the flame at 5 cm above the burner.

An uncertainty analysis was performed, consisting of calculation of individual uncertainty components and root mean square summation of components. All uncertainties are reported as *expanded uncertainties*: $X \pm ku_c$, from a combined standard uncertainty (estimated standard deviation) u_c, and a coverage factor $k = 2$. Likewise, when reported, the relative uncertainty is ku/X. The expanded relative uncertainties for the experimentally determined quantities in this study are 4% for the volume fractions of CO_2.

3. Computational methods

A time-dependent, axisymmetric numerical code (UNICORN) [17] solves the axial and radial (z and r) full Navier–Stokes momentum equations, continuity, and enthalpy- and species-conservation equations on a staggered-grid system. The body-force term due to the gravitational field is included in the axial-momentum equation to simulate upward-oriented flames. A clustered mesh system is employed to trace the gradients in flow variables near the flame surface. A detailed reaction mechanism of GRI-Mech-V1.2 [18] for methane–oxygen combustion (31 species and 346 elementary reactions) is incorporated into UNICORN. Thermophysical properties of species are calculated from the polynomial curve fits for 300–5000 K. Mixture viscosity and thermal conductivity are then estimated using the Wilke and Kee expressions, respectively. A simple, optically thin-media, radiative heat-loss model [19] for CO_2, H_2O, CH_4, and CO, is incorporated into the energy equation.

[1] Certain commercial equipment, instruments, or materials are identified in this paper to adequately specify the procedure. Such identification does not imply recommendation or endorsement by NIST or NASA, nor does it imply that the materials or equipment are necessarily the best available for the intended use.

The finite-difference forms of the momentum equations are obtained using an implicit QUICKEST scheme [20], and those of the species and energy equations are obtained using a hybrid scheme of upwind and central differencing. At every time-step, the pressure field is accurately calculated by solving all the pressure Poisson equations simultaneously and using the LU (Lower and Upper diagonal) matrix-decomposition technique.

Calculations are made on a physical domain of 200 mm by 47.5 mm using a 251×101 or 541×251 non-uniform grid system that yields a minimum grid spacing of 0.2 mm by 0.2 mm or 0.05 mm by 0.05 mm, respectively, in both the z and r directions in the flame zone. A flame-base oscillating condition is obtained with the coarse grid by adding CO_2 to coflow incrementally, followed by the oscillating flame calculation with the fine grid. No artificial perturbations are necessary to establish the periodic vortices and base oscillations. The integration time was 100 and 25 μs for the coarse and fine grid systems, respectively. The computational domain is bounded by the axis of symmetry and a chimney wall boundary in the radial direction and by the inflow and outflow boundaries in the axial direction. Flat velocity profiles are imposed at the fuel and air inflow boundaries, while an extrapolation procedure with weighted zero- and first-order terms is used to estimate the flow variables at the outflow boundary. The burner outer diameter is 28 mm and the chimney inner diameter is 95 mm. The burner wall (1-mm long and 1-mm thick) temperature is set at 600 K. The mean fuel and oxidizer velocities are $U_F = 0.921$ and $U_o = 10.7$ cm/s [13–15], respectively.

4. Results and discussion

4.1. Experimental observations

The methane coflow diffusion flame anchored at the burner rim and inclined inwardly as a result of the stream-tube shrinkage due to flow acceleration by buoyancy as well as considerably low fuel velocity compared to that of the coflowing air [21]. The flame was flickering with occasional flame-tip separation. Figure 1 shows the measured flame flickering frequency (f) as a function of the mean oxidizer (air) velocity (U_o). The flickering frequency increased with an increase in U_o and exhibited a bimodal nature; it jumped from ≈11 Hz to ≈15 Hz, at U_o ≈11 cm/s and shifted down to the lower mode at U_o ≈15 cm/s. The sudden transition in the flickering frequency under a constant U_o suggested that the scale of the vortices changed.

As CO_2 was added to air, the flame base detached from the burner rim toward the downstream direction (upward and inward). By approaching the flame extinguishment limit, the flame base oscillated radially and, at a lesser extent, axially. Figure 2 shows consecutive color video images (30 Hz) of nearly one cycle of the flame-base oscillation in a methane flame in the air with CO_2 added at a volume fraction of $X_a \approx 0.158$. The intensity of the blue flame base was brighter when moving outward (Figs. 2e and f) than inward (Figs. 2a–d).

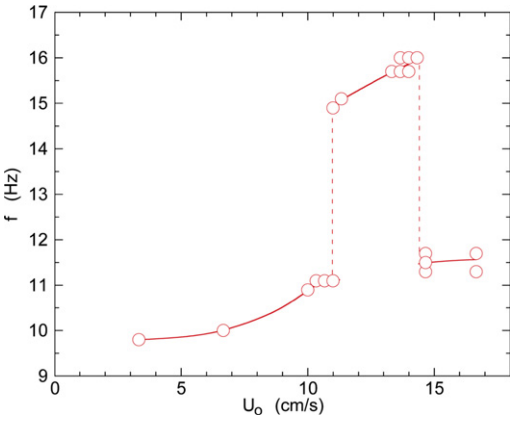

Fig. 1. Measured flame-flickering frequency as a function of the mean oxidizer (air) velocity. $U_F = 0.92$ cm/s.

Figure 3 shows the temporal variations of the axial and radial flame-base co-ordinates (z_f and r_f, respectively) from the burner exit plane and the centerline determined from video footage during which X_a was gradually increased toward blowoff. The frequency of the flame-base oscillation was approximately 6 Hz. The flame-base movement determined from the right- and left-hand sides were in synchronization; i.e., axisymmetric. The amplitude of oscillations increased gradually with time and ultimately, the flame could not re-attach and blew off as z_f exceeded ≈6 mm.

4.2. Numerical simulations

The flame flickering and extinguishment characteristics in the cup burner were reported, in detail, elsewhere [13–15]. The numerical simulation predicted the flame-flickering frequency in methane flames in air as ≈11 Hz in good agreement with the experimental observation. The flame-base oscillation was simulated numerically as well. Figure 4 shows a time sequence (0.03-s interval) of the calculated temperature and heat-release rate contours in an oscillating methane diffusion flame in air with CO_2 at $X_a = 0.14$. The predicted extinguishment was at $X_a = 0.143$–0.145 [13,21], which was ≈9% lower than the measured value of $X_a = 0.157$ [21]. The evolution and development of buoyancy-induced vortices in the

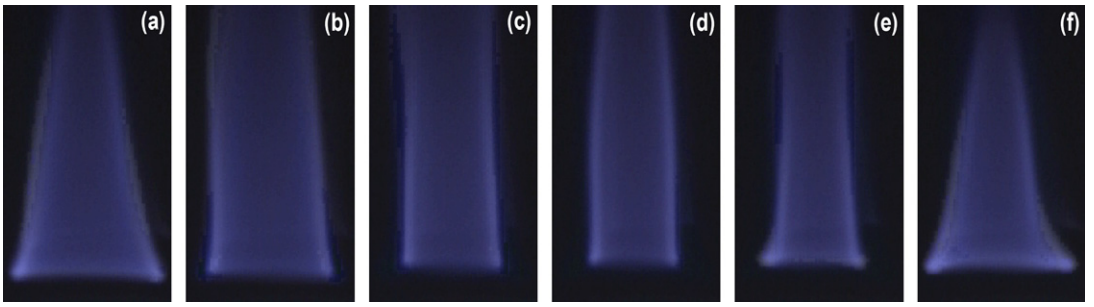

Fig. 2. Consecutive video images (30 Hz) of an oscillating methane flame in air with CO_2. $U_F = 0.92$ cm/s, $U_o = 6.7$ cm/s, $X_a \approx 0.158$. Image width: ≈25 mm; burner exit plane ≈ bottom edge of image.

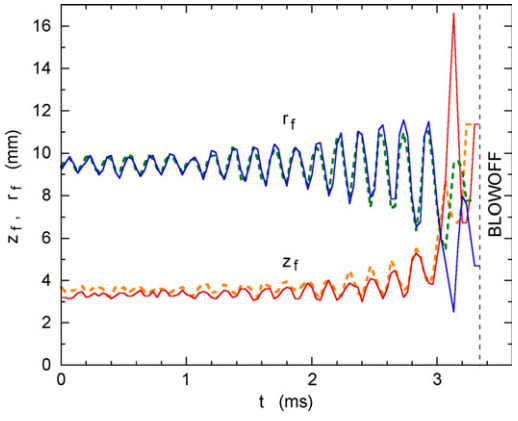

Fig. 3. Measured flame-base location in an oscillating methane flame in air with CO_2. Solid, right edge; dashed, left edge.

near field resulted in wavy isotherms and the flame zone, i.e., flame flickering.

The flame base traveled one cycle of oscillation in approximately 0.16 s (≈6 Hz), during which two vortices evolved and thus the flame-flickering frequency was ≈12 Hz. When the flame base anchored at the burner rim (Fig. 4a), a vortex evolved and grew large (Figs. 4b–f) by entraining the oxidizer. On the other hand, when the flame base was at the innermost location (Fig. 4d), another vortex evolved to form a small vortex (Figs. 4e and f) because of minimal entrainment. The flame tip separation was also simulated (Figs. 4b and f), when the vortex squeezed out the bulk of the fuel to form a separated flame island at the tip.

Figure 5 shows the calculated near-field structure of a methane flame in air with CO_2 ($X_a = 0.14$) at three different elapse times ($t = 0.03$, 0.09, and 0.12 s). The origin of the elapse time ($t = 0$) was arbitrarily chosen at an attached-flame condition (Fig. 4a), which was obtained after calculations of a few oscillation cycles. The variables include the velocity vectors (v), isotherms (T), total heat-release rate ($\dot{q}$), and the local equivalence ratio (ϕ_{local}) [12] on the right; the total molar flux vectors of atomic hydrogen ($\mathbf{M}_H$), oxygen volume fraction (X_{O_2}), oxygen consumption rate ($-\hat{\omega}_{O_2}$), and mixture fraction (ξ) [22], including stoichiometry ($\xi_{st} = 0.045$), on the left.

As was reported in the earlier papers [23–26], the reaction kernel (a peak reactivity [$\dot{q}$ or $-\hat{\omega}_{O_2}$] spot) formed in the flame base stabilizes the trailing diffusion flame downstream. Because of dilution of the oxidizer by CO_2, the reaction rates were reduced, and therefore, the flame base was susceptible to small velocity fluctuations. As a vortex was generated outside the flame zone near the burner exit (Fig. 5a; see bulges in T and ξ and **v**), the velocity of the entrainment flow into the flame-stabilizing region increased, and thus the flame base drifted inwardly. The oxygen penetrated onto the fuel side, forming a high oxygen concentration zone around the flame base. The chain radicals (H, OH, and O) formed at high temperatures diffused on both sides of the flame zone and, at the flame base, downward into the oxygen-rich zone (Fig. 5a; see M_H), thus enhancing the chain-branching reaction, $H + O_2 \rightarrow OH + O$, and subsequent radical reactions to form the reaction kernel. The heat-release rate, oxygen consumption rate, velocity, temperature, oxygen volume fraction, local equivalence ratio, and mixture fraction at the reaction kernel were $\dot{q}_k = 120$ J/cm^3 s, $-\hat{\omega}_{O_2,k} = 0.00034$ mol/cm^3 s, $|\mathbf{v}_k| = 0.322$ m/s $T_k = 1485$ K, $X_{O_2,k} = 0.043$, $\phi_{local} = 0.71$, and $\xi_k = 0.040$, respectively.

As the flame base reached the innermost position (Fig. 5b), the buoyancy-driven entrainment velocity toward the flame base decreased because the bulk of hot vortex passed downstream. A large fuel–air mixing space was formed between the flame base and the burner rim in the wake, and thus the oxygen penetration onto the fuel side progressed further. The values at the reaction kernel were $\dot{q}_k = 130$ J/cm^3 s, $-\hat{\omega}_{O_2,k} = 0.00036$ mol/cm^3 s, $|\mathbf{v}_k| = 0.215$ m/s $T_k = 1469$ K, $X_{O_2,k} = 0.047$, $\phi_{local} = 0.67$, and $\xi_k = 0.039$.

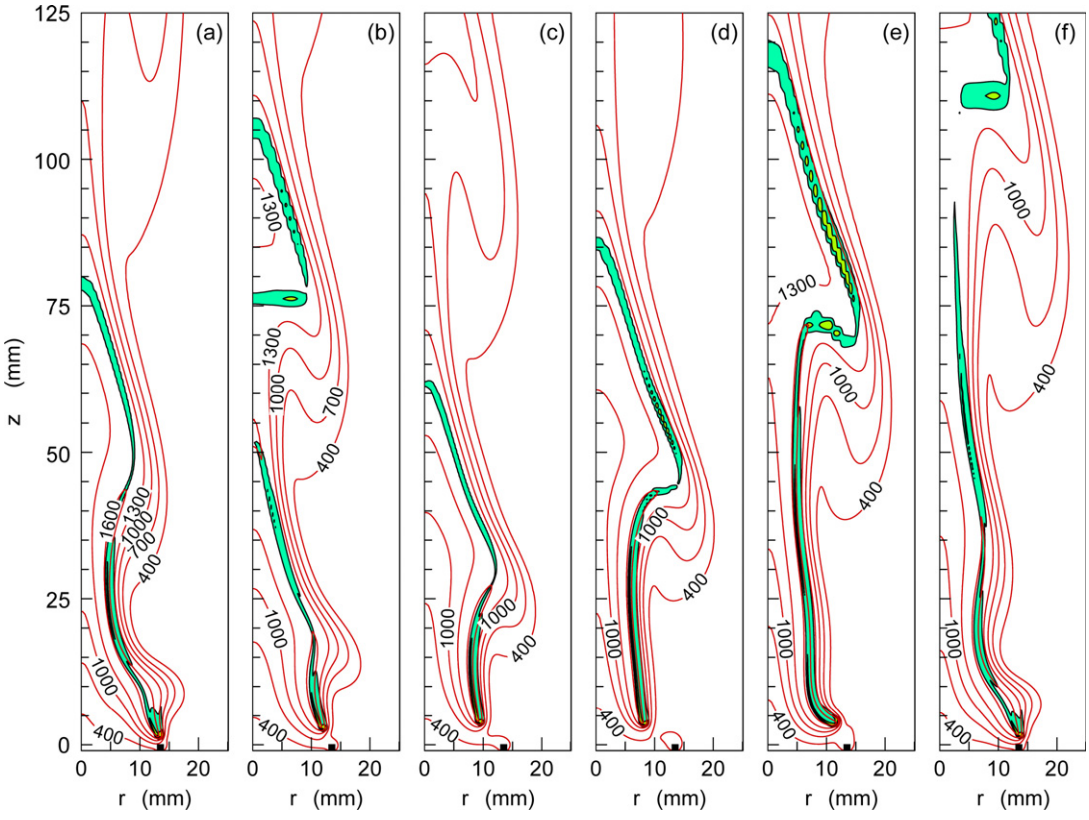

Fig. 4. Calculated temperature and heat-release rate (5, 20, and 100 J/cm^3 s) contours in an oscillating methane flame in air with CO_2. $U_F = 0.92$ cm/s, $U_o = 10.7$ cm/s, and $X_a \approx 0.14$. Time interval: 0.03 s.

As the flammable mixture layer with a sufficient thickness was established in the low-speed wake region and ignited, the edge diffusion flame propagated back outwardly (Fig. 5c) toward the burner rim. The reaction kernel was broadened perpendicularly to propagation and its structure resembled that of a propagating flame through a mixing layer formed in a fuel jet studied previously [12]. The triple flame structure was not formed for methane flames as reported previously [12]. As the flame base consumed the mixture and reached the burner radius, it turned downward toward the burner rim, returning to the attached flame position. A new vortex evolved and these processes repeated. Therefore, the flame-base oscillation is coupled with the buoyancy-induced vortex generation (and flame flickering).

Figure 6 shows the temporal variations in the properties at the reaction kernel: the axial and radial coordinates (z_k, r_k), the total flame transit velocity and components ($|\mathbf{v}_f|$, U_f, V_f), determined from the slopes of z_k, and r_k, respectively, the total flow velocity and components ($|\mathbf{v}_k|$, U_k, V_k), the relative velocity ($|\mathbf{v}_k - \mathbf{v}_f|$), the temperature ($T_k$), the heat-release rate ($\dot{q}_k$), and the heat-release rate to velocity ratios ($\dot{q}_k/|V_k|, \dot{q}_k/|\mathbf{v}_k - \mathbf{v}_f|$) in the methane flame in air with CO_2. The last quantities represent ratios of the residence time and the reaction time, or the local evaluation of the Damköhler number [24], thus indicating the flame strength. One cycle of the flame-base oscillation can be divided into three phases: flame drifting, propagation, and settling. In the flame drifting phase (approximately $t = 0$–0.09 s), the flame base detached from the burner rim and drifted upward and inward by the entrainment flow. The relative velocity ($|\mathbf{v}_k - \mathbf{v}_f|$), determined from the velocity components, increased initially, while the total flow velocity ($|\mathbf{v}_k|$) varied moderately. The reciprocal of the former must represent the residence time more accurately than that of the latter because the flame base was moving. As the heat-release rate remained nearly constant during this phase, $\dot{q}_k/|\mathbf{v}_k - \mathbf{v}_f|$ decreased gradually, indicating flame weakening. The temperature remained almost constant (≈1480 K) throughout the cycle. In the flame propagation phase (approximately $t = 0.09$–0.14 s), the flammable mixture ignited and the flame base moved back toward the burner rim. The heat-release rate increased from 130 to 206 J/cm^3 s and the relative velocity quadrupled during this phase. The ratio, $\dot{q}_k/|\mathbf{v}_k - \mathbf{v}_f|$, doubled immediately at the ignition of the flammable mixture and then decreased. The flame propagation

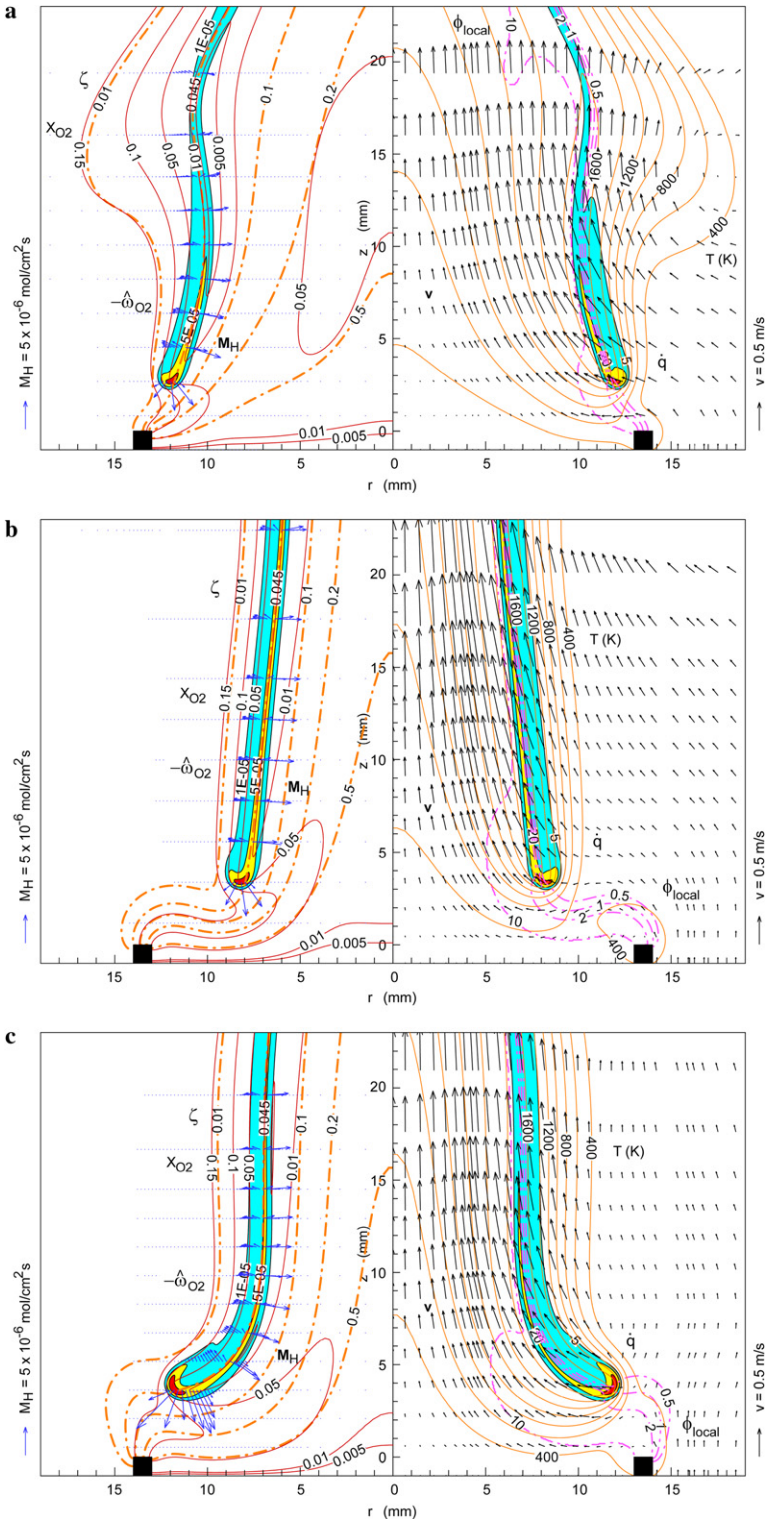

Fig. 5. Calculated structure of an oscillating methane flame in air with CO_2: (a) drifting phase, (b) innermost point, and (c) propagating phase. $U_F = 0.92$ cm/s, $U_o = 10.7$ cm/s, and $X_a = 0.14$. Elapse time (arbitrary zero for Fig. 4a): (a) 0.03 s, (b) 0.09 s, and (c) 0.12 s.

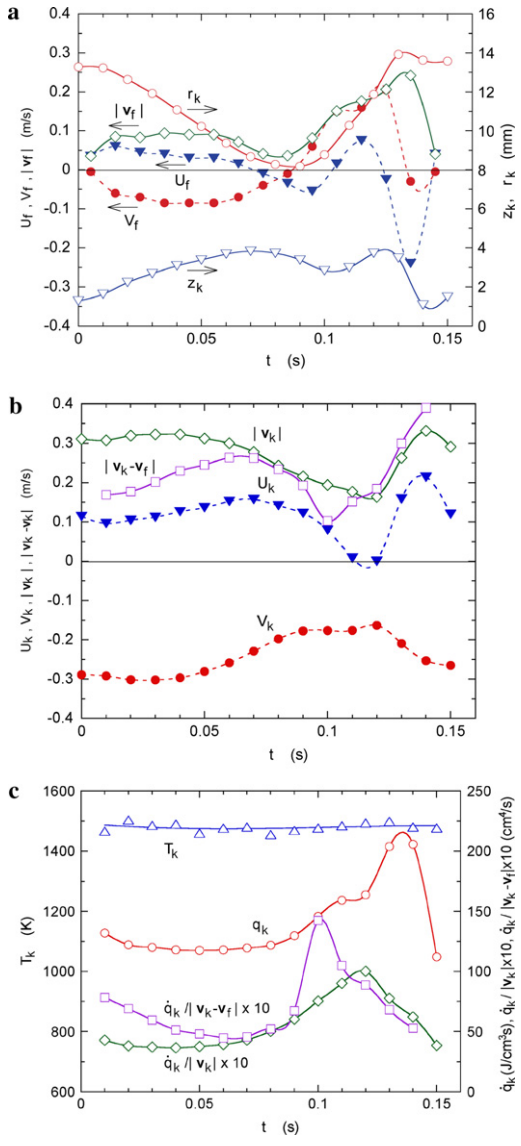

Fig. 6. Temporal variations in the reaction kernel properties: (a) location, flame transit velocity, (b) flow velocity, (c) temperature, and heat-release rate in a methane flame in air with CO_2.

phase was followed by the short settling phase (approximately $t = 0.14$–0.16 s), in which the flame structure rapidly returned to the attached flame conditions.

Figure 7 shows the heat-release rate and the ratio, $\dot{q}_k/|\mathbf{v}_k - \mathbf{v}_f|$. The lower branch corresponds to the flame drifting phase and the upper branch was the flame propagation branch. The reaction kernel weakened (decreasing $\dot{q}_k/|\mathbf{v}_k - \mathbf{v}_f|$) during the flame drifting phase, but the transition to the upper branch occurred as the flammable mixture layer ignited. Although $\dot{q}_k$ increased during the flame propagation phase, $|\mathbf{v}_k - \mathbf{v}_f|$ increased more

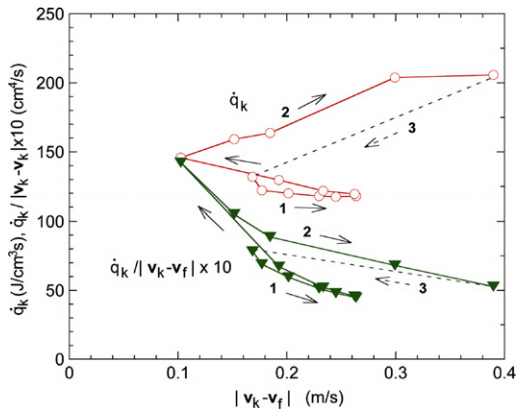

Fig. 7. Heat-release rate and the ratio with relative velocity: 1, drifting phase, 2, propagation phase, and 3, settling phase.

rapidly and the reaction kernel weakened. If the ignition of the mixture did not occur, the flame base drifted further downstream, i.e., blowoff.

5. Conclusions

The experimental observations and numerical simulations with full chemistry have revealed the unsteady flame structure and the oscillation behavior of edge diffusion flames of methane in coflowing air with CO_2. Bi-modal flame-flickering frequencies of ≈11 Hz or ≈15 Hz were observed, depending on the coflow velocity. The computation predicted the flame flickering at the lower frequency mode and the edge oscillation at half the flickering frequency in good agreement with the experiment. The flame-base oscillation occurred in three phases: flame drifting, propagation, and settling. The flame drifting phase lasted ≈0.09 s, during which the edge diffusion flame detached from the burner rim, drifted downstream, and the fuel–air flammable mixture layer was formed. In the flame propagation phase, the flammable mixture ignited and the flame returned to the burner rim in ≈0.05 s, followed by the short (≈0.02 s) settling phase, in which the flame structure returned to the attached flame conditions. The relatively long fuel–air mixing time required before the edge diffusion flame propagation occurs implies that the relatively slow molecular diffusion process to form the flammable mixture layer may limit the probability of propagation of locally quenched flamelets in turbulent flames.

Acknowledgment

This work was supported by the Office of Biological and Physical Research, National Aeronautics and Space Administration, Washington, DC.

References

[1] F.A. Williams, *Combustion Theory*, second ed., Benjamin/Cummings, Menlo Park, California, 1985, p. 408.
[2] T. Pressing, P. Terheven, N. Peters, M.S. Mansour, *Combust. Flame* 115 (1998) 335–353.
[3] J. Backmaster, N. Peters, *Proc. Combust. Inst.* 21 (1986) 1829–1836.
[4] J.S. Kim, *Combust. Theory Modelling* 1 (1997) 13–40.
[5] U. Hegde, M.Y. Bahadori, D.P. Stocker, AIAA Paper, 99-0582 (1999).
[6] M. Füri, P. Papas, P.A. Monkewitz, *Proc. Combust. Inst.* 28 (2000) 831–838.
[7] H. Sato, K. Amagi, M. Arai, *Proc. Combust. Inst.* 28 (2000) 1981–1987.
[8] S.H. Won, S.H. Chung, M.S. Cha, B.J. Lee, *Proc. Combust. Inst.* 28 (2000) 2093–2099.
[9] S. Kukuck, M. Matalon, *Combust. Theory Modelling* 5 (2001) 217–240.
[10] J. Kim, S.H. Won, M.K. Shin, S.H. Chung, *Proc. Combust. Inst.* 29 (2002) 1589–1595.
[11] S.H. Won, J. Kim, M.K. Shin, S.H. Chung, O. Fujita, T. Mori, J.H. Choi, K. Ito, *Proc. Combust. Inst.* 29 (2002) 37–44.
[12] F. Takahashi, V.R. Katta, *Proc. Combust. Inst.* 30 (2005) 375–382.
[13] V.R. Katta, F. Takahashi, G.T. Linteris, in: *Fire Safety Science: Proceedings of the Seventh International Symposium, International Association for Fire Safety Science*, 2003, pp. 531–544.
[14] V.R. Katta, F. Takahashi, G.T. Linteris, *Combust. Flame* 137 (2004) 506–522.
[15] G.T. Linteris, V.R. Katta, F. Takahashi, *Combust. Flame* 138 (2004) 78–96.
[16] Anon., "Standard on Clean Agent Fire Extinguishing Systems," National Fire Protection Association, NFPA 2001, Quincy, MA, 2000.
[17] W.M. Roquemore, V.R. Katta, *Proc. VSJ-SPIE98*. Yokohama, Japan, Paper No. KL310, 1998.
[18] M., Frenklach, H. Wang, M. Goldenberg, G.P. Smith, D.M. Golden, C.T. Bowman, R.K. Hanson, W.C. Gardiner, V. Lissianski, *GRI-Mech—An Optimized Detailed Chemical Reaction Mechanism for Methane Combustion*, Technical Report No. GRI-95/0058, Gas Research Institute, Chicago, Illinois, 1995.
[19] Anon., *Computational Submodels, International Workshop on Measurement and Computation of Turbulent Nonpremixed Flames*, http://www.ca.sandia.gov/TNF/radiation.html, 2003.
[20] V.R. Katta, L.P. Goss, W.M. Roquemore, *AIAA J.* 32 (1994) 84.
[21] F. Takahashi, G.T. Linteris, V.R. Katta, *Proc. Combust. Inst.* 31 (2006) (in press).
[22] R.W. Bilger, *Proc. Combust. Inst.* 22 (1988) 475.
[23] F. Takahashi, V.R. Katta, *Proc. Combust. Inst.* 27 (1998) 675–684.
[24] F. Takahashi, V.R. Katta, *Proc. Combust. Inst.* 28 (2000) 2071–2078.
[25] F. Takahashi, V.R. Katta, *Proc. Combust. Inst.* 29 (2002) 2509–2518.
[26] F. Takahashi, V.R. Katta, *Proc. Combust. Inst.* 30 (2005) 383–390.

Comments

Satya Chakravarthy, IIT Madras, India. I am not clear about where the upstream boundary of your computational domain is and what boundary condition is applied there. Particularly, are you including a part of the burner rim into the computational domain and considering the oscillating convective heat loss that would occur to the burner material, which could affect the flame oscillations?

Reply. The upstream boundary is located 1 mm below the burner-exit plane. The burner rim is thus inside the computational domain and assumed to be at a constant temperature (600 K). Because the flame-base oscillation is strongly coupled with the buoyancy-driven vortex evolution, the effect of the oscillating heat loss to the burner on the flame oscillation would be minor.

•

Thierry Poinsot, CNRS, France. Did you check mesh independency? For GRI-mech, radicals like H_2O_2 or HO_2 require high resolution. Did you look at the fields of such species?

Reply. We did not check mesh independency systematically. However, we used a coarse mesh system (200 μm minimum grid spacing) to obtain an oscillating flame solution and then switched to a fine mesh system (50 μm minimum grid spacing) to gain more detailed internal structure of the oscillating flame. In our previous study [1], in which 50-μm grid spacing was used, the calculated transit velocity of propagating edge diffusion flames equaled to the measured laminar flame speed of the stoichiometric fuel–air mixture. The result implies that the concentration and reaction rate fields of species that are critical for premixed-type flame propagation (including H_2O_2 and HO_2) have been resolved with a sufficient accuracy.

Reference

[1] F. Takahashi, V.R. Katta, *Proc. Combust. Inst.* 30 (2005) 375–382.